ELSEVIER

Journal of Nuclear Materials 275 (1999) 81–94

journal of nuclear materials

www.elsevier.nl/locate/jnucmat

^{79}Se: geochemical and crystallo-chemical retardation mechanisms

Fanrong Chen [a,c], Peter C. Burns [b], Rodney C. Ewing [a,*]

[a] *Department of Nuclear Engineering and Radiological Sciences, The University of Michigan, Ann Arbor, MI 48109-2104, USA*
[b] *Department of Civil Engineering and Geological Sciences, University of Notre Dame, Notre Dame, IN 46556-0767, USA*
[c] *Guangzhou Institute of Geochemistry, Chinese Academy of Sciences, Wushan, Guangzhou 510640, People's Republic of China*

Received 12 January 1999; accepted 15 March 1999

Abstract

^{79}Se is a long-lived (1.1×10^6 yrs) fission product which is chemically and radiologically toxic. Under Eh–pH conditions typical of oxidative alteration of spent nuclear fuel, selenite, SeO_3^{2-} or $HSeO_3^-$ or selenate, SeO_4^{2-}, are the dominant aqueous species of selenium. Because of the high solubility of metal-selenites and metal-selenates and the low adsorption of selenite and selenate aqueous species by geological materials under alkaline conditions, selenium may be highly mobile. However, ^{79}Se released from altered fuel may become immobilized by incorporation into secondary uranyl phases as low concentration impurities, and this may significantly reduce the mobility of selenium. Analysis and comparison of the known structures of uranyl phases indicate that (SeO_3) may substitute for (SiO_3OH) in structures of α-uranophane and boltwoodite that are expected to be the dominant alteration products of UO_2 in Si-rich groundwater. The substitutions (SeO_3) ↔ (SiO_3OH) in sklodowskite, $Mg[(UO_2)(SiO_3OH)]_2(H_2O)_6$ and (SeO_3) ↔ (PO_4) in phurcalite, $Ca_2[(UO_2)_3(PO_4)_2O_2](H_2O)_7$, may occur with the eliminated apical anion being substituted for by an H_2O group, but experimental investigation is required. The close similarity between the sheets in the structures of rutherfordine, $[(UO_2)(CO_3)]$ and $[(UO_2)(SeO_3)]$ implies that the substitution (SeO_3) ↔ (CO_3) can occur in rutherfordine, and possibly other uranyl carbonates. However, the substitutions: (SeO_3) ↔ (SiO_4) in soddyite and (SeO_3) ↔ (PO_4) in phosphuranylite may disrupt their structural connectivity and are, therefore, unlikely.

1. Introduction

Selenium is essential to humans, animals and some plants and has a narrow concentration range between deficient and toxic levels in the diets of humans and animals [1,2]. Moreover, ^{79}Se is a long-lived fission product with a half-life of 1.1×10^6 yrs and is chemically and radiologically toxic. Because of the high mobility of selenium in oxidizing geochemical environments, the behavior of selenium is important in safety analyses of radioactive waste repositories.

A recent sensitivity analysis [3] based on an illustrative performance assessment analysis of a disposal concept for nuclear waste has shown that ^{79}Se can have a significant effect on the cumulative radioactive dose if it is transported through the geosphere without retardation. Based on recent performance assessments of the proposed repository at Yucca Mountain [4,5], it is clear that ^{79}Se and a limited number of other relatively long-lived radionuclides make the dominant contributions to final dose calculations (e.g., the transuranium elements: ^{237}Np, ^{239}Pu and fission products: ^{79}Se, ^{99}Tc and ^{129}I). We note that these previous performance assessments have been based on an erroneous half-life of 65 000 yrs for ^{79}Se. A recent measurement gives a corrected half-life of 1.1×10^6 yrs [6]; thus, there may be even greater contributions of ^{79}Se to the longer term dose estimates.

Solubility-controlled precipitation and adsorption by geological and engineered materials are generally considered as important retardation mechanisms for radionuclides. However, uranyl phases form as alteration products during the oxidative dissolution of spent nuclear fuel [7–11], and the uranyl alteration products may

* Corresponding author.

0022-3115/99/$ - see front matter
PII: S0022-3115(99)00105-1

become host phases for radionuclides released from the altered spent nuclear fuel [11–13]. Thus, the mobility of ^{79}Se released from the corroded UO_2 may be significantly reduced by Se incorporation into the structures of the secondary uranyl phases. We have previously reported on the incorporation of actinides into the uranyl phases [13]. An analysis of the incorporation of ^{99}Tc into uranyl phases is in progress [14]. In addition to geochemical retardation mechanisms, we report, in this paper, on the atomic-scale incorporation of ^{79}Se into the alteration phases formed during corrosion of UO_2 under oxidizing conditions.

2. Speciation and solubility of selenium

2.1. Speciation

Selenium can occur in natural systems in different oxidation states: selenide(2−), elemental Se(0), selenite(4+) and selenate(6+), and the selenium of each oxidation state may occur as a number of different species in solution. Experimental and theoretical studies have demonstrated that the mobility of selenium decreases as the selenium is reduced from Se(6+) to Se(0) and Se(2−). Therefore, selenium mobility and availability in water–rock (soil) systems is dependent on the speciation, which is mainly determined by the reduction–oxidation reactions.

The surface composition of spent nuclear fuel during dissolution has the general formula UO_{2+x}, where the value of x is 0 to 0.33 under the Eh conditions that are achievable in an underground repository [15,16]. Thus, the Eh–pH conditions for the oxidative alteration of spent fuel will be in the stability field of uranyl phases relative to that of UO_{2+x} ($0 \leqslant x \leqslant 0.33$). However, the paragenesis of the secondary uranyl phases (uranyl oxyhydroxides, silicates, phosphates, carbonates and vanadates) depends largely on the composition of the groundwater [17,18]. The alteration paragenesis revealed in nature analogue studies can be used to describe the alteration products of spent fuel under similarly oxidizing environment. For example, the Nopal I uranium deposit in the Peña Blanca district in Chihuahua, Mexico, is located in a crystalline terrain and has a geochemical environment similar to that at the proposed high level nuclear waste repository at Yucca Mountain [19]. The uranyl mineral paragenetic sequence of Nopal I deposit is similar to that observed in other uranium deposits [17]. Schoepite initially forms during the early stage of oxidative alteration of uraninite and is then followed and replaced by uranyl silicates, mainly α-uranophane and soddyite [19]; becquerelite was identified by X-ray diffraction (XRD) analysis but not observed by optical microscopy. Thus, the stability fields for uranophane, soddyite and becquerelite with respect to UO_{2+x} ($0 \leqslant x \leqslant 0.33$) in the UO_2–CaO–SiO_2–H_2O system can be used to predict the Eh–pH conditions for the oxidative alteration of spent nuclear fuel. Assuming the Si and Ca concentrations are similar to those in the J-13 groundwater at Yucca Mountain (Table 1), the calculated stability relations between the uranyl phases and UO_{2+x} are shown in Fig. 1. Because of the high silica concentration in Yucca Mountain J-13 groundwater, becquerelite is a metastable phase with respect to soddyite and uranophane; thus it is not included in Fig. 1. The field above the equilibrium lines between the uranyl phases and UO_{2+x} represents the probable conditions for the oxidative alteration of spent fuel in a repository for which oxidizing conditions prevail. The Yucca Mountain J-13 groundwater has a higher salinity as compared with the groundwater in other igneous rock areas (Table 1); however, the groundwater composition has limited influence on the calculated stability relations. For example, if the Si concentration is one order of magnitude lower, the Eh value of the stability boundaries between uranyl phases and UO_{2+x} will shift 40 to 90 mV higher than that shown in Fig. 1. Thus, the compositional variation of groundwaters listed in Table 1 will not result in appreciable change of the stability relations shown in Fig. 1.

Fig. 2 illustrates the distribution of selenium species as a function of Eh–pH, with reference to the stability relations between the uranyl phases and UO_{2+x}. The dissolved selenium is most probably a selenite species during the oxidative alteration of spent fuel. Under

Table 1
Mean composition of Yucca Mountain J-13 groundwater [20] and some groundwater-derived surface water in primarily igneous rock areas [21] (mg/l)

	J-13	Groundwater-derived surface water				
		1	2	3	4	5
Li	0.042					
Na	43.9	3.3	4.2	8.4	5.95	2.07
K	5.11	1.2	1.2	2.2	1.57	0.59
Ca	12.5	5.8	4.6	8.3	10.4	4.8
Mg	1.92	2.4	1.3	3.7	1.7	1.54
Sr	0.035					
Al	0.012					
Fe	0.006					
Si	27.0	5.37	7.05	21.6	11.49	8.73
F	2.2					
Cl	6.9	3.4	2.6	4.2	1.06	0.6
HCO_3^-	125.3	15.9	12.2	43.9	54.6	24.0
SO_4^-	18.7	10.9	3.7	0.8	2.38	1.1
pH	7.6	6.1	7.7	7.1	6.8	6.3

1. Vosges, France (after thawing, 1967); 2. Central Massif, France (after several dry months, summer 1967); 3. Senegal (in eastern regions, dry season in 1967); 4. Sierra Nevada, California (1961); 5. Kenora, NW Ontario (Piezometers in glacial sands derived from granitic Precambrian rocks).

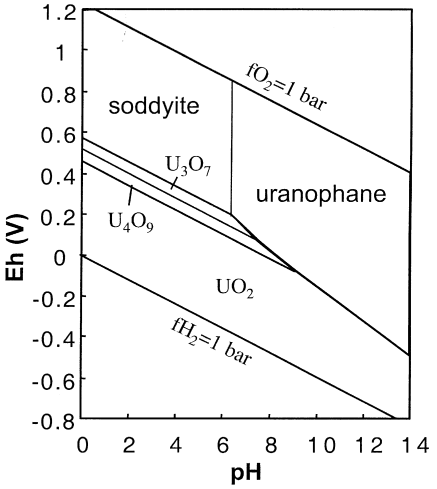

Fig. 1. Eh vs. pH diagram showing the stability relations among uranium phases equilibrated with Yucca Mountain J-13 groundwater. The thermodynamic data for UO_{2+x} are from Grenthe et al. [22], and those for soddyite and uranophane are from Chen et al. [23].

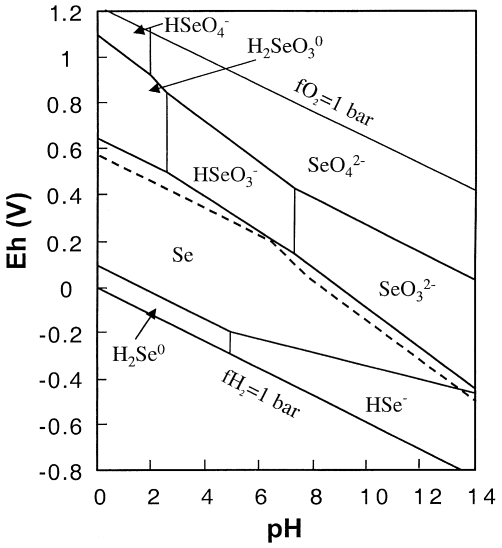

Fig. 2. pH vs Eh predominance diagram for the aqueous species of selenium. The dashed line represents the equilibrium between uranyl phases and UO_{2+x} as illustrated in Fig. 1. The field above the dashed line represents the probable conditions for the oxidative alteration of spent fuel. The thermodynamic data for selenium species are from Wagman et al. [29].

more oxidizing conditions, SeO_4^{2-} can be significant. In addition, adsorption experiments by Fujikawa and Fukui [24] have demonstrated that oxidation of selenite to selenate is promoted in the presence of sorbents, i.e., there was a positive correlation between the fraction of selenate in solution and the fraction of Se adsorbed, when the selenium was first added into the solution as selenite.

2.2. Solubility

During the oxidative dissolution of spent nuclear fuel, Se concentrations in the near-field will be enhanced due to the release of radioactive ^{79}Se from the oxidized fuel. However, if the concentration of selenite species is high enough, some selenite phase may precipitate. Therefore, the solubility of selenite compounds can be used to constrain the upper limit of the concentration of selenium in the near-field. Because of the much higher solubility of selenates than selenite, precipitation of selenate compounds is not expected, and thus will not be discussed.

Because the availability and mobility of selenium in soils have long been an important subject of environmental research, thermodynamic data for a large number of metal selenites have been obtained by experimental studies and empirical estimations [25–27]. As an example, if the concentration of the metal ions in the near-field solutions is not significantly different from that in Yucca Mountain J-13 groundwater, precipitation of $CaSeO_3 \cdot nH_2O$, $MgSeO_3$ and $Fe_2(OH)_4SeO_3$ is probable. Assuming that the concentrations of calcium, magnesium and iron in near-field solutions are equal to those in J-13 groundwater and that all of the iron in the solution is Fe(3+), the solubility-limited Se concentrations with respect to these metal–selenites can be calculated as a function of pH (Fig. 3). Calcium species considered in the calculation include Ca^{2+}, $Ca(OH)_2^0$ and $CaSeO_3^0$; magnesium species include Mg^{2+}, $Mg(OH)_2^0$ and $MgSeO_3^0$; iron species include Fe^{3+}, $Fe(OH)^{2+}$, $Fe(OH)_2^+$, $Fe(OH)_3^0$, $Fe(OH)_4^-$. Also shown in Fig. 3 are

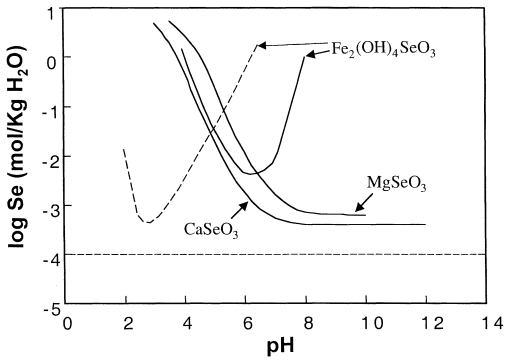

Fig. 3. Metal-selenite solubility-limited Se concentrations in aqueous solution which have the same calcium, magnesium and iron concentrations as J-13 groundwater. The dashed line represents $Fe_2(OH)_4SeO_3$ solubility-limited Se-concentrations as calculated assuming the Fe^{3+} concentration is controlled by the solubility of amorphous $Fe(OH)_3$.

the solubility-limited Se concentrations with respect to $Fe_2(OH)_4SeO_3$ based on the assumption that the Fe^{3+} concentrations in the aqueous solution are controlled by the solubility of amorphous $Fe(OH)_3$, which is most probably the case in the near-field due to the corrosion of steel canisters. The Se concentration determined by the solubility of $Fe_2(OH)_4SeO_3$ has a minimum under acidic conditions in both cases (pH = 6.5, Se = 4.54×10^{-3} m; pH = 3, Se = 4.83×10^{-4} m, respectively), while those determined by the solubility of $CaSeO_3 \cdot nH_2O$ and $MgSeO_3$ approach their lower limits of 3.94×10^{-4} m and 6.31×10^{-4} m, respectively, under alkaline conditions. The lower limits of the metal-selenite solubility-limited Se concentrations are several orders of magnitude higher than the 10 μg/l ($\sim 1.27 \times 10^{-7}$ m) and 400 mg/l ($\sim 5.06 \times 10^{-6}$ m) permitted, respectively, in drinking and waste water [28]. The lower concentration of Ca and Mg in groudwaters from other igneous rock areas will result in higher solubility of Se in groundwater.

Moreover, uranyl selenites may occur as secondary alteration phases. There are 13 known uranyl selenites, but no solubility or thermodynamic data are available for these phases. Considering that uranyl selenite minerals are rare in nature and often associated with uranyl silicates, especially high concentration of aqueous Se may be necessary for the precipitation of these minerals.

3. Adsorption of selenite and selenate

Selenium is expected to be in the form of selenite and, perhaps, selenate in the geochemical environments associated with the oxidative alteration of spent nuclear fuel. Because the solubility-limited Se concentrations with respect to metal selenites are high, immobilization mechanisms other than solubility limits are necessary to reduce the ^{79}Se concentration in the near-field. Sorption of ^{79}Se by backfill and geological materials may be important. Selenite adsorption is similar to that of PO_4^{3-} and is generally thought to occur by ligand exchange [30,32]. Selenite forms an inner-sphere complex with the hydrolyzed surface of the sorbants. However, selenate is only weakly adsorbed and does not form inner-sphere complexes [33]. Both mononuclear and binuclear complexes may exist for chemisorption mechanisms of SeO_3^{2-} on oxide and mineral surfaces [34]. There are many factors affecting the sorption of selenite, of which the influence of sorbent composition and solution pH are the most important.

Selenite adsorption by Fe oxides is extensive, rapid, and decreases as pH increases [30,35,36]. John et al. [37], in a study of 66 New Zealand soils, concluded that, in general, selenite adsorption increased as the extent of soil weathering increased. The amount of selenite adsorbed was best correlated with oxolate-extractable Fe, but significant positive correlations were also found with organic C content and extractable Al and Si. The 1:1 layer-type clay, kaolinite, exhibits greater adsorption capacity than the 2:1 minerals, vermiculite and montmorillonite [38,39], but selenite sorption by clays is affected to a greater extent by pH than by the layer-type of clays. The influence of sorbents on selenite sorption results from the differences in their adsorbing surfaces. Parfitt [31] has shown that the ligand-exchange mechanism is applicable to both metal hydrous oxides and phyllosilicates and Rajan [40] has interpreted data on the adsorption of selenite by hydrous alumina at pH 5 as evidence for the preferential adsorption of the SeO_3^{2-} species on highly positive sites. Weathered forms of Fe, Al and Si were hypothesized to be the active sites for selenite adsorption [41], while the rather high selenite adsorption capacity of phyllosilicates is considered to result from the presence of reactive adsorption sites at the edge surfaces of broken crystallites and on the exposed surfaces of adsorbed hydroxy polymers [31].

The significant influence of pH on SeO_3^{2-} adsorption has been demonstrated by numerous authors [34,41–44]. Se sorption experiments by Bar-Yosef and Meek [39] using 5×10^{-3} m $CaCl_2$ solution with a Se concentration of 0.316 μm/l demonstrated that almost all the dissolved Se in a 35 ml solution could be adsorbed by 4 g of kaolinite at pH = 4, but 85% of the total Se was found in the solution after the 35 ml solution was equlibriated with 4 g kaolinite at pH = 8. A similar pH influence on Se sorption by montmorillonite has also been demonstrated. Thus, adsorption under alkali conditions is not expected to be an effective retardation mechanism for selenite. It has been proposed that at a low pH, a protonated surface was produced on the adsorbant which attracts the selenium anions and decreases OH^- competition for adsorption sites [24,34]. Bar-Yosef and Meek [39] have suggested that the effect of pH on selenite adsorption results mainly from modifying the anion's adsorption capacity.

Anion competition for adsorption sites also influences Se adsorption. Increasing PO_4^{3-} in solution decreases SeO_3^{2-} adsorption [45]. Comparisons between the Se sorption results of kaolinite and montmorillonite [39] and the data on P adsorption on kaolinite [46] and B adsorption on Na–montmorillonite [47] indicate that at a similar solution concentration and pH, Se sorption was approximately 30 times lower than P and four times greater than B. Assuming that the three anions share the same adsorption sites, it is reasonable to expect elevated Se concentration in soil solutions, due to orthophosphate fertilization. This effect was indeed reported for a soil under laboratory conditions by Geering et al. [48]. Fujikawa and Fukui [24] have made comparisons for anion (SO_4^{2-}, Cl^-, CO_3^{2-}, HCO_3^-) competition with the selenite anion for adsorption sites and concluded that SO_4^{2-} was the most effective competitor. Finally, all

experimental data have shown that selenite sorption consists of a fast process followed by a slow process [34,39]. The fast process is usually accomplished in less than a couple of days and accounts for more than 90% of the total sorption.

In order to describe or predict adsorption of anions, such as SeO_3^{2-}, equilibrium adsorption models are often employed. The Freundich and Langmuir models have been used to describe the relationship between the sorbed anion and solution concentration of the anion. The relationships often produce predictions very close to what is observed experimentally, although the relationships are not as valid at lower concentrations of adsorbate [49]. Bar-Yosef and Meek [39] displayed a satisfactory description of Se adsorption by kaolinite and montmorillonite using the modified competitive Langmuir adsorption equation [47] within the Se concentration range of 0–12 μm/l and pHs between 4 and 8, which covers the pH and Se concentration in most Se-affected drainage water. Recent results by Baylock et al. [34] showed a significant deviation from the Freundich isotherm, and a clear relationship between the selenite concentration and the adsorbed selenite was not evident. Thus, the application of the initial mass isotherm to predict Se adsorption was proposed. These model studies and correlations provide some insight into selenite adsorption by different geological materials and have a heuristic value, but it is evident that the quantitative, predictive models for selenium adsorption by near-field geological materials and back-fill clays are still lacking.

4. Incorporation of selenite and selenate into uranyl phases

Under the oxidizing, alkaline conditions that are expected to occur in the near-field of a nuclear waste repository [50,51], selenium is highly soluble and not expected to be adsorbed effectively by geological or backfill materials. The incorporation of trace amounts of Se into the structures of the uranyl phases that form by alteration of UO_2 may have a profound impact upon the release rates of Se from the near-field. In the event that these phases incorporate significant amounts of Se, they become the source term for Se.

4.1. Crystal chemistry of U^{6+}

The structures of uranyl minerals are exceptionally diverse, due largely to the complex crystal chemistry of U^{6+}. The U^{6+} cation almost invariably occurs in crystal structures as part of a nearly linear $(UO_2)^{2+}$ uranyl ion (designated Ur), with U^{6+}–O_{Ur} bond-lengths of ~0.179 nm [52]. The uranyl ion has a formal valence of 2+, and as such, it must be coordinated by anions in a crystal structure. The uranyl ion is coordinated by four, five or six approximately coplanar anions (Fig. 4), forming $Ur\phi_4$ square bipyramids, $Ur\phi_5$ pentagonal bipyramids and $Ur\phi_6$ hexagonal bipyramids (ϕ: O^{2-}, OH^-), respectively. The U^{6+}-ϕ_{eq} bond-lengths are dependent upon the number of coordinating anions, and average 0.228(5), 0.237(9) and 0.247(12) nm for $Ur\phi_4$, $Ur\phi_5$ and $Ur\phi_6$ polyhedra, respectively, in numerous well-refined structures [52].

Typical bond-valencies at each ligand in uranyl polyhedra are provided in Fig. 4, as calculated using the average polyhedral geometries from well-refined structures and the bond-valence parameters provided by Burns et al. [52]. The uranyl-ion oxygen atom receives ~1.7 valence units (vu) from the U^{6+}–O_{Ur} bond, thus the bonding requirements of the O_{Ur} anions are largely satisfied without substantial further bonding. The O_{Ur} anions may bond to low-valence cations or accept hydrogen bonds, but they cannot bond to cations of higher bond-valence. The situation is rather different for the equatorial ligands (Fig. 4), which only have ~0.5 vu from the U^{6+} cation at the center of the polyhedra. These anions require substantial additional bonding to satisfy their bond-valence requirements and will commonly bond to cations of higher bond-valence. As such, it is common for uranyl polyhedra to polymerize with other uranyl polyhedra, or other cation polyhedra of higher bond-valence, but this polymerization invariably involves either the sharing of equatorial edges or equatorial corners of the uranyl polyhedra, and never the apical (O_{Ur}) ligands. The strongly asymmetric distribution of bond valences within the uranyl polyhedra results in polymerization that is dominantly in two dimensions, most often resulting in sheets of polyhedra of higher bond-valence, but also sometimes resulting in chains and finite clusters of polyhedra. Burns et al. [53] established a structural hierarchy for 180 uranyl phases that is based upon the polymerization of those polyhedra of higher bond-valence. The hierarchy contains classes corresponding to structures that are based upon sheets, chains, finite clusters, and frameworks of

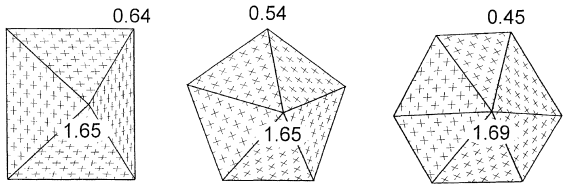

Fig. 4. The types of uranyl polyhedra that occur in crystal structures, and the typical bond valences incident upon the ligands due to the bond to U^{6+} at the center of the polyhedron. The bond valences were calculated for the average bond-lengths of numerous polyhedra from well-refined structures using the bond-valence parameters provided by Burns et al. [52]. (a) Uranyl square bipyramid, (b) pentagonal square bipyramid, (c) hexagonal square bipyramid.

polyhedra of higher bond-valence, as well as a few structures that do not involve polymerization of polyhedra of higher bond-valence.

4.2. Crystal chemistry of Se^{4+} and Se^{6+}

Under oxidizing conditions, Se may occur as either Se(4+) or Se(6+), resulting in the dominance of either the selenite, $(SeO_3)^{2-}$, or the selenate, $(SeO_4)^{2-}$. Owing to electronic effects, the crystal–chemical behavior of these two species is substantially different (Fig. 5). In the case of selenate, the Se^{6+} cation is tetrahedrally coordinated (Fig. 5(a)), and the typical Se^{6+}–O bond-length, from sums of effective ionic radii [54], is 0.164 nm. In selenite, however, the Se^{4+} cation is electron lone-pair stereoactive, resulting in a one-sided coordination polyhedron that contains three co-planar anions, with the cation displaced above the anion plane (Fig. 5(b)). Inspection of structures containing selenite (Table 2) indicates that the Se^{4+}–O bond-length is ~0.170 nm.

No uranyl selenate minerals are known. Six uranyl selenite minerals have been described, and the crystal structures have been determined for guilleminite [55], demesmaekerite [56] and derriksite [57] (Fig. 6). The structure of guilleminite contains sheets of uranyl and selenite polyhedra (Fig. 6(a)) that are based upon the phosphuranylite anion-topology [53] shown in Fig. 6(b). The topology contains triangles, squares, pentagons and hexagons and is the basis for the sheets that occur in twelve structures, most of which contain uranyl phosphate sheets. In the guilleminite sheet, the pentagons and hexagons in the anion topology are populated by uranyl ions, giving pentagonal and hexagonal bipyramids, respectively. The triangles in the topology contain the selenite group, and the squares remain empty. The interlayer

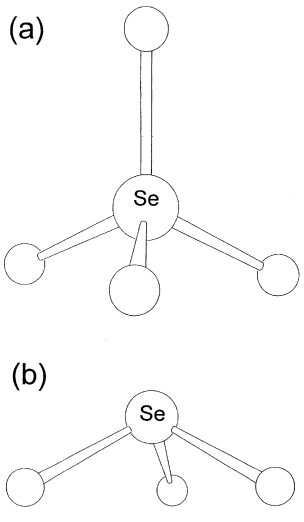

Fig. 5. Typical geometries of (a) selenate and (b) selenite.

of the structure contains Ba which is coordinated by ten anions, one is an equatorial ligand of the uranyl polyhedra, six are O_{Ur} anions of adjacent sheets, and three are (H_2O) groups that are located in the interlayer. The structure of piretite, $Ca(UO_2)_3(SeO_3)_2(OH)_4(H_2O)_4$ [58], is probably closely related to, or isostructural with, guilleminite, although a structure determination has not been done owing to the lack of suitable crystals.

The structures of demesmaekerite and derriksite are both based upon the infinite chains of polymerized polyhedra of higher bond-valence, although the chains are quite different. The derriksite chain (Fig. 6(d)) contains $Ur\phi_4$ square bipyramids that share all equatorial ligands with selenite polyhedra, and each selenite group shares two ligands with adjacent uranyl polyhedra. The structure also contains Cu polyhedra, but these are not part of the chain. The demesmaekerite chain (Fig. 6(c)) contains $Ur\phi_5$ pentagonal bipyramids that share corners with selenite groups. There are two types of selenite groups; those that bridge between adjacent uranyl polyhedra in the chain, and thus share two ligands with uranyl polyhedra, and those that are attached to the side of the chain by sharing a single ligand with a uranyl polyhedron. The structure of demesmaekerite also contains Pb and Cu polyhedra.

The crystal structures of two synthetic uranyl selenite phases are known (Table 2). Perhaps the most interesting of these is the structure of $[(UO_2)(SeO_3)]$ [59], which has a structure that is closely related to rutherfordine, $[(UO_2)(CO_3)]$ [60]. Both structures have sheets of polyhedra that are based upon the rutherfordine anion-topology which contains both hexagons and triangles (Fig. 7(a)–(b)). The hexagons are populated with uranyl ions, giving hexagonal bipyramids, and the triangles are populated with either (SeO_3) or (CO_3). The sheets are linked through van der Waals forces only. The structure of $[(UO_2)(HSeO_3)_2(H_2O)]$ [61] contains a chain of uranyl and selenite polyhedra that is related to the chain observed in demesmaekerite. The chain contains $Ur\phi_5$ pentagonal bipyramids that are linked by sharing edges with selenite groups, with all selenite groups two-connected to the chain (Fig. 7(c)); the selenite groups that are one-connected to similar chains in the structure of demesmaekerite do not occur in this structure. Adjacent chains are linked through hydrogen bonds to interstitial (H_2O) groups.

The structures of two uranyl selenate phases have been reported (Table 2). The phase $[(UO_2)(SeO_4)(H_2O)_2](H_2O)_2$ [63] contains chains of corner-sharing $Ur\phi_5$ pentagonal bipyramids and selenate tetrahedra (Fig. 8(a)), with the polyhedra arranged such that each $Ur\phi_5$ pentagonal bipyramid shares three corners with selenate tetrahedra, and each selenate tetrahedra links to three adjacent $Ur\phi_5$ pentagonal bipyramids. Identical chains have been observed in several other structures that contain chromate or sulfate tetrahedra, rather than

Table 2
Interatomic distances between X (Se^{4+}, Se^{6+} Si^{4+}, P^{5+}) and O^{2-} in uranyl structures

Name	Formula	X–O (nm)				Ref.
	UO_2SeO_4	0.163	0.165	0.192	0.163	[62]
	$[UO_2SeO_4(H_2O)_2]$ $(H_2O)_2$	0.164	0.163	0.163	0.161	[63]
	$(NH_4)[(UO_2)F(SeO_4)](H_2O)$	0.157	0.165	0.169	0.169	[64]
	UO_2SeO_3	0.169	0.173	0.173		[59]
	$(UO_2)(HSeO_3)_2(H_2O)$	0.167	0.169	0.176		[61]
demesmaekerite	$Pb_2Cu_5[(UO_2)(SeO_3)_3]_2(OH)_6(H_2O)_2$	0.171	0.168	0.169		[56]
		0.169	0.168	0.171		
		0.172	0.169	0.173		
derriksite	$Cu_4[(UO_2)(SeO_3)_2](OH)_6$	0.164	0.170	0.170		[57]
		0.165	0.170	0.170		
	$(UO_2)(Se_2O_5)$	0.164∼	0.168∼	0.180∼		[65]
		0.166	0.170	0.182		
	$(NH_4)(UO_2)(HSeO_3)(SeO_3)$	0.169	0.170	0.170		[66]
		0.168	0.168	0.174		
guilleminite	$Ba[(UO_2)_3(SeO_3)_2O_2](H_2O)_3$	0.167	0.168	0.171		[55]
α-uranophane	$Ca[(UO_2)(SiO_3OH)]_2(H_2O)_5$	0.160	0.161	0.163	0.164	[67]
sklodowskite	$Mg[(UO_2)(SiO_3OH)]_2(H_2O)_6$	0.161	0.163	0.163	0.165	[68]
boltwoodite	$K[(UO_2)(SiO_3OH)](H_2O)$	0.153	0.160	0.162	0.162	[69]
kasolite	$Pb[(UO_2)(SiO_4)](H_2O)$	0.159	0.162	0.164	0.168	[70]
soddyite	$(UO_2)_2(SiO_4)(H_2O)_2$	0.164	0.164	0.164	0.164	[71]
meta-autunite	$Ca[(UO_2)(PO_4)]_2(H_2O)_8$	0.146	0.146	0.146	0.146	[72]
phosphuranylite	$KCa(H_3O)_3(UO_2)[(UO_2)_3(PO_4)_2O_2]_2$ $(H_2O)_8$	0.151	0.154	0.154	0.154	[73]
phurcalite	$Ca_2[(UO_2)_3(PO_4)_2O_2](H_2O)_7$	0.151	0.154	0.155	0.155	[74]
dumonite	$Pb_2[(UO_2)_3(PO_4)_2O_2](H_2O)_5$	0.149	0.151	0.154	0.155	[75]
dewindtite	$Pb_3[H(UO_2)_3(PO_4)_2O_2]_2(H_2O)_{12}$	0.152	0.153	0.153	0.155	[76]
upalite	$Al[(UO_2)_3(PO_4)_2O(OH)](H_2O)_7$	0.151	0.152	0.154	0.154	[77]
françoisite	$Nd[(UO_2)_3(PO_4)_2O(OH)](H_2O)_6$	0.153	0.155	0.156	0.156	[78]
phuraluminite	$Al_2[(UO_2)_3(PO_4)_2(OH)_2](OH)_4(H_2O)_{10}$	0.152	0.154	0.156	0.156	[79]
althupite	$AlTh(UO_2)[(UO_2)_3(PO_4)_2O(OH)]_2$ $(OH)_3(H_2O)_{15}$	0.148∼0.153	0.151∼0.154	0.155∼0.157	0.156∼0.159	[80]

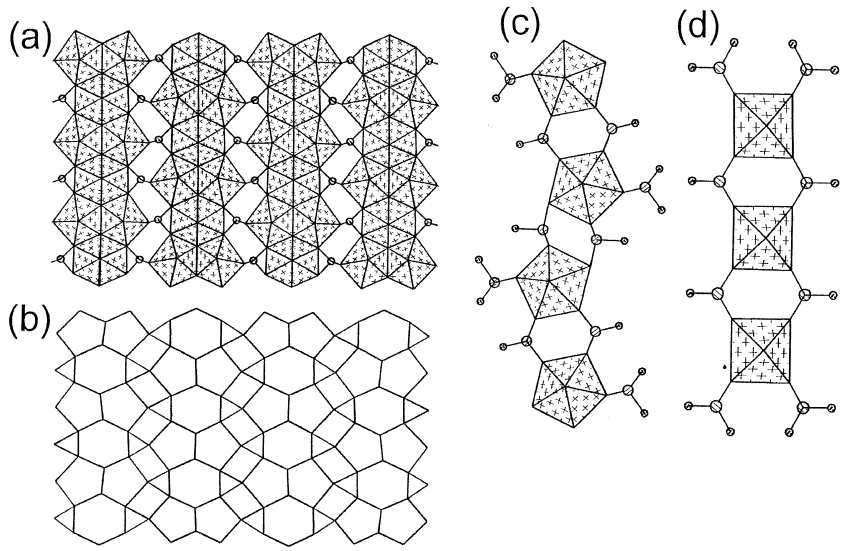

Fig. 6. Structural units that occur in uranyl selenites. (a) The sheet in guilleminite, (b) the phosphuranylite anion-topology, (c) the chain in demesmaekerite, (d) the chain in derriksite. Uranyl polyhedra are shaded with crosses, selenium atoms are shown as circles shaded with parallel lines.

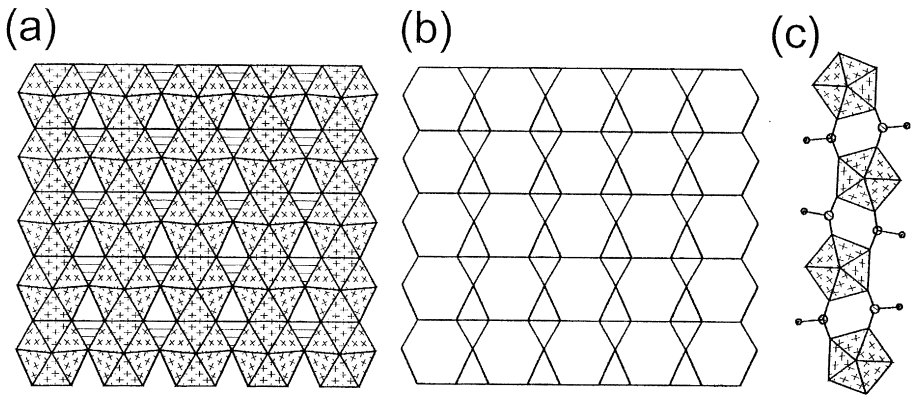

Fig. 7. Structural units that occur in uranyl selenites. (a) The sheet that occurs in $[(UO_2)(SeO_3)]$ and rutherfordine, (b) the rutherfordine anion-topology, (c) the chain that occurs in $[(UO_2)(HSeO_3)_2(H_2O)]$. Legend as in Fig. 6.

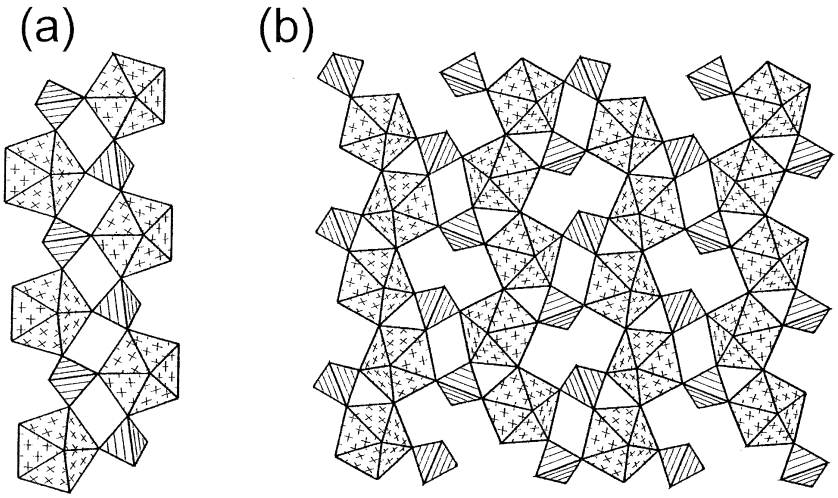

Fig. 8. The structural units that occur in uranyl selenates. (a) The chain that occurs in $[(UO_2)(SeO_4)(H_2O)_2](H_2O)_2$. (b) the sheet that occurs in $(NH_4)[(UO_2)F(SeO_4)](H_2O)$.

selenate [53]. The structure of $(NH_4)[(UO_2)F(SeO_4)](H_2O)$ [64] is based upon infinite sheets of corner-sharing $Ur\phi_5$ pentagonal bipyramids and selenate tetrahedra (Fig. 8(b)). In both of the uranyl selenate structures that are known, the selenate tetrahedra share only corners with uranyl polyhedra. This is consistent with the observation [52] that those polyhedra that contain cations with valences of 6+ (with the exception of U^{6+}) tend not to share edges with uranyl polyhedra; where polymerization of polyhedra of higher bond-valence occurs in such cases, it is by the sharing of polyhedral corners only.

4.3. Possible incorporation mechanisms

According to natural analogue studies [17,19,81], the primary alteration phases of UO_2 under oxidizing conditions will be uranyl oxide hydrates, as well as alkali and alkaline earth uranyl oxide hydrates. Continued alteration leads to the formation of uranyl silicates, uranyl phosphates, or uranyl carbonates, depending upon the composition of the water that contacts the spent fuel. Here we investigate the likelihood of the incorporation of Se into each of these mineral groups.

4.3.1. Uranyl oxide hydrates

On the basis of natural analogue studies [17,19,81] and laboratory experiments [7–11,82,83] the minerals ianthinite, schoepite, becquerelite, compreignacite and billietite are likely to form due to the corrosion of spent nuclear fuel under oxidizing conditions. The formulas of these minerals are given in Table 2. Each of these structures contain uranyl polyhedra that share edges to form sheets, with low-valence cations and (H_2O) groups

located in interlayer positions [52,53,84]. Both selenite and selenate are polyhedra of higher bond-valence, and as such, are likely to polymerize with uranyl polyhedra as part of the structural unit, rather than occurring as interlayer constituents. Thus, it is unlikely that either will be incorporated to any significant extent into the structures of the uranyl oxide hydrates.

4.3.2. Uranyl silicates

Of the 15 known uranyl silicates, boltwoodite, sklodowskite, α-uranophane, soddyite and haiweeite have been identified as phases that may form due to the corrosion of spent nuclear fuel in a Si-rich environment [9,83]. The formulas for each of these minerals are given in Table 3. Of these, the structures of boltwoodite, sklodowskite and α-uranophane all contain topologically identical sheets of $Ur\phi_5$ pentagonal bipyramids and acid silicate tetrahedra (Fig. 9(a)). The sheet is based upon the uranophane anion-topology [53] (Fig. 9(b)) which contains chains of edge-sharing pentagons that are connected through chains of alternating edge-sharing triangles and squares. This anion topology is the basis of 16 structures; in all but one case, all pentagons of the anion topology are populated by uranyl ions, giving $Ur\phi_5$ pentagonal bipyramids, and either the triangles or the squares of the anion topology are populated, but never both in the same structure.

Table 3
Uranyl phases found as alteration products of UO_2 and spent nuclear fuel

Structure known	
schoepite	$[(UO_2)_8O_2(OH)_{12}](H_2O)_{12}$
becquerelite	$Ca[(UO_2)_3O_2(OH)_3]_2(H_2O)_8$
compreignacite	$K_2[(UO_2)_3O_2(OH)_3]_2(H_2O)_8$
billietite	$Ba[(UO_2)_3O_2(OH)_3]_2(H_2O)_4$
soddyite	$(UO_2)_2(SiO_4)(H_2O)_2$
Na–boltwoodite	$(Na,K)(H_3O)[(UO_2)(SiO_4)]$
sklodowskite	$Mg[(UO_2)(SiO_3OH)]_2(H_2O)_6$
uranophane	$Ca[(UO_2)(SiO_3OH)]_2(H_2O)_5$
Structure not known	
dehydrated schoepite	$UO_3(H_2O)_{0.8-1.0}$
haiweeite	$Ca(UO_2)_2Si_6O_{15}(H_2O)_5$

Is it possible that selenite can substitute in the structures of any of the uranyl silicates that may form when spent fuel is altered? First, consider the structures with α-uranophane-type sheets (α-uranophane, boltwoodite and sklodowskite). The only plausible substitution into these structures is $(SeO_3) \leftrightarrow (SiO_3OH)$. In these cases, the O^{2-} anions of the acid silicate group are bonded to U^{6+} cations within the sheet; whereas, the apical $(OH)^-$ anions are only bonded to one Si^{4+} cation within the sheet. The base of the (SeO_3) groups in the structures of guilleminite, demesmaekerite and derriksite have O–O distances in the range 0.256–0.265 nm. This may be compared to the ideal edge-length of 0.264 nm for a (SiO_4) tetrahedron, calculated assuming a bond angle of 109.4° and a Si–O bond-length of 0.162 nm. (Table 2). Thus, on the basis of geometrical similarity, the (SeO_3) group is well suited to substitute for (SiO_3OH) in the α-uranophane-type sheet. However, there is also the issue of charge balance. The incorporation of a hydrogen atom, perhaps as part of a hydronium ion in the interlayer, or a minor variation of occupancy of the interlayer cation positions could provide charge balance. Thus, if the $(OH)^-$ groups of the acid silicate groups are not required to maintain structural connectivity, the substitution $(SeO_3) \leftrightarrow (SiO_3OH)$ may occur.

According to Ginderow [67], there are two symmetrically distinct acid silicate groups in the structure of α-uranophane. The hydrogen atom in one of these (SiO_3OH) groups connects to an interlayer (H_2O) group

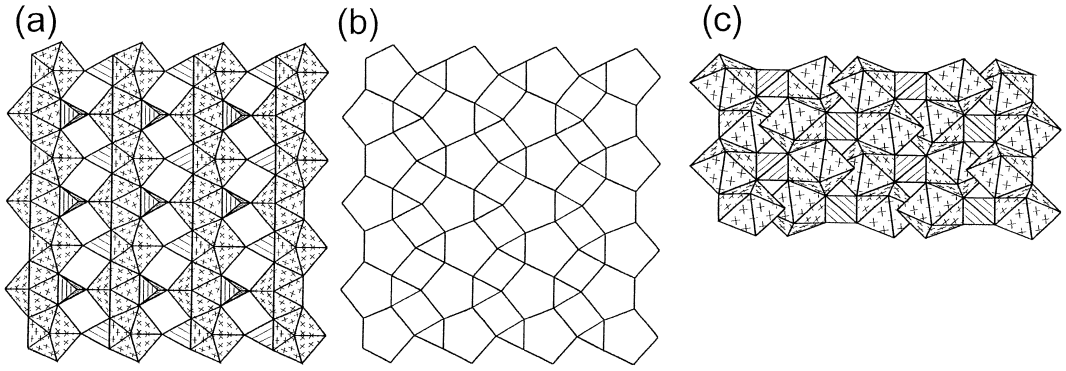

Fig. 9. Structural units in uranyl silicate minerals. (a) The α-uranophane-type sheet that occurs in the structures of α-uranophane, sklodowskite and boltwoodite, (b) the uranophane anion-topology, (c) the framework structure of soddyite. Uranyl polyhedra are shaded with crosses and silicate tetrahedra are shaded with parallel lines.

via a weak hydrogen bond with a distance of 2.20 Å, and the oxygen atom of the $(OH)^-$ group accepts a somewhat stronger hydrogen bond that is donated from an interlayer (H_2O) group, with a bond length of 0.182 nm. The substitution $(SeO_3) \leftrightarrow (SiO_3OH)$ would disrupt both of these hydrogen bonds, but a redistribution of hydrogen bonds locally in the structure could occur, and substitution of trace amounts of (SeO_3) would likely not destabilize the structure significantly. The $(OH)^-$ anion of the other acid silicate group is bonded to an interlayer Ca cation with a Ca–OH (OH: the oxygen anion of the $(OH)^-$ groups) bond-valence of 0.29 vu. The Ca coordination polyhedron includes two O_{Ur} anions (one from each adjacent sheet), one $(OH)^-$ group that is part of the acid silicate group, and four (H_2O) groups. In addition, the interlayer contains an 'isolated' (H_2O) group that is held in the structure by hydrogen bonding only and is bonded as a hydrogen bond acceptor to the $(OH)^-$ group bonded to the Ca cation. Because the bond-valence of a Ca–OW (OW = the oxygen in H_2O groups) in the structure is 0.27 to 3.4 vu, the substitution of an H_2O group for the $(OH)^-$ group bonded to a Ca cation can satisfy the bond-valence requirement of the cation. Therefore, when the $(OH)^-$ is eliminated due to the substitution $(SeO_3) \leftrightarrow (SiO_3OH)$, the oxygen anion in the H_2O group that would have been bonded as a hydrogen bond acceptor to the $(OH)^-$ group may be bonded to the Ca cation with a redistribution of hydrogen bonds locally in the structure. As such, the substitution $(SeO_3) \leftrightarrow (SiO_3OH)$ coupled with the substitution $H_2O \leftrightarrow (OH)^-$ would probably occur, although it is more likely for (SeO_3) to substitute at the other tetrahedral sites.

In the structure of sklodowskite [68], all the $(OH)^-$ groups in the acid silicate group are bonded to the Mg cation in the interlayer. Of the anions coordinating the Mg cation, two are oxygens of the $(OH)^-$ anions from (SiO_3OH) groups, four are oxygen anions from water groups. There are two more water molecules per empirical formula unit that are held in the interlayer by hydrogen bonds only. The bond-valences of the Mg–OH and Mg–OW bonds are 0.31 and 0.41 vu, respectively, which indicates that the substitution of a Mg–OW bond for a Mg–OH bond can satisfy the bond-valence requirement of the Mg cation, and the structural connectivity would not be disrupted. This indicates that (SeO_3) may be incorporated into the structure of sklodowskite as an impurity by the substitution $(SeO_3) \leftrightarrow (SiO_3OH)$ coupled with the substitution of an isolated H_2O group for an $(OH)^-$ group, but experimental verification is required.

Boltwoodite shows substantial substitution of Na for K [85], and the Na analogue of boltwoodite has been described as a mineral species [86]. The Na cation is octahedrally coordinated by four O_{Ur} anions and two (H_2O) groups; whereas, the K cation is coordinated by four O_{Ur} anions, the $(OH)^-$ group that is part of the acid silicate group, as well as two (H_2O) groups. There is only one symmetrically unique acid silicate group in the structure, and the apical $(OH)^-$ group is bonded to an interlayer K cation with a bond length of 0.325 nm. This bond is rather weak and is most probably not essential for the stability of the structure. The hydrogen positions have not been determined for the structure, but the $(OH)^-$ group presumably also participates in hydrogen bonds with interlayer (H_2O) groups. It is significant that Na cations do not assume the same positions as K cations in the interlayer [85] and that the $(OH)^-$ group is not bonded to the Na cation when it is present. Thus, substitution of Na for K in the interlayer may enhance $(SeO_3) \leftrightarrow (SiO_3OH)$ substitution.

The structure of soddyite consists of a framework of $Ur\phi_5$ pentagonal bipyramids and silicate tetrahedra [71] (Fig. 9(c)). The $Ur\phi_5$ pentagonal bipyramids share edges to form chains that are cross-linked to chains both above and below by sharing edges with silicate tetrahedra. Because the silicate tetrahedra share each of their corners with $Ur\phi_5$ uranyl polyhedra, it is unlikely that the substitution $(SeO_3) \leftrightarrow (SiO_4)$ can occur in soddyite, as this would disrupt the structural connectivity.

Finally, the crystal-chemical behavior of selenate is very similar to that of sulfate. Burns et al. [52] noted that those polyhedra that contain cations with the valence 6+ (with the exception of U^{6+}) seldom share an edge with a uranyl polyhedra. This principle is well demonstrated by the structures of synthetic uranyl selenate phases (Fig. 8, see above). Each of the silicate tetrahedra in the structures of α-uranophane, boltwoodite, sklodowskite and soddyite involve the sharing of an edge with a uranyl polyhedron, and as such, the substitution of selenate for silicate in any of these structures is unlikely.

4.3.3. Uranyl phosphates

The structures of uranyl phosphate minerals are dominated by uranyl phosphate sheets that are based upon the phosphuranylite anion-topology which is shown in Fig. 10(a). The sheets are derived from the phosphuranylite anion-topology by populating each pentagon and hexagon with a uranyl ion, giving $Ur\phi_5$ pentagonal and $Ur\phi_6$ hexagonal bipyramids, respectively, and the triangles are the faces of tetrahedra (Fig. 10(b)–(d)). In each of these sheets the tetrahedra share an edge with the $Ur\phi_6$ hexagonal bipyramid and the opposite corner with a $Ur\phi_5$ pentagonal bipyramid. The apical ligand of the tetrahedra only bond to P within the sheet. These sheets differ only in the orientation of the tetrahedra. The interlayer composition among the phases with the phosphuranylite anion-topology (Table 2) is quite different. This indicates that the local bond-valence can be satisfied by the adjustment of the interlayer composition in the structure. As discussed above, the structure of guilleminite, a uranyl selenite,

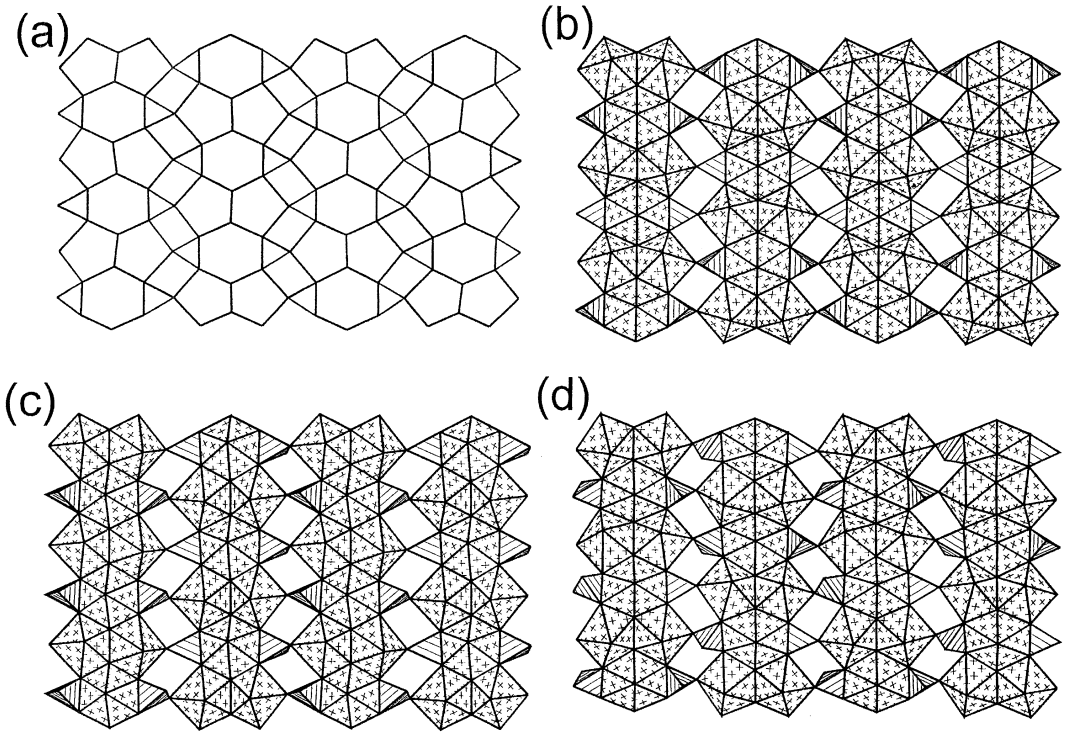

Fig. 10. Structural units in uranyl phosphate minerals. (a) The phosphuranylite anion-topology, (b) the sheet that occurs in phosphuranylite, upalite, françoisite, and dewindtite, (c) the sheet that occurs in vanmeersscheite and dumontite, (d) the sheet that occurs in phurcalite, phuralumite, and althupite.

contains sheets that are also based upon the phosphuranylite anion-topology, with (SeO_3) groups populating the triangles of the anion topology, rather than (PO_4) tetrahedra. This observation implies that the substitution (SeO_3) $\leftrightarrow$ (PO_4) is possible, if structural connectivity is not disrupted by the elimination of an anion apice due to the substitution.

In the structures of uranyl phosphate minerals, the apical (non-sheet) anions of the phosphate tetrahedra are invariably bonded to an interlayer cation. However, if the apical ligand eliminated by the substitution (SeO_3) $\leftrightarrow$ (PO_4) can be substituted for by a water group without disrupting the structural connectivity, the substitution may occur. In the structure of phurcalite [74], there are two symmetrically different (PO_4) tetrahedra. The apical anions denoted as O(22) and O(23), respectively, in each of the two kinds of (PO_4) tetrahedra are bonded to the interlayer Ca cation with an approximate bond-valence of 0.33 to 0.46 vu. Each of the Ca cations is coordinated by 7 or 8 anions, of which 3 or 4 are oxygen anions in water groups. The isolated H_2O group denoted as W(29) is held in the structure by hydrogen bonds only. The cation-OW bond valence is usually about 0.4 vu [87] and is about 0.3 vu in the structure of phurcalite. This implies that the substitution of the isolated water group W(29) for O(22) may also satisfy the bond-valence requirement of the cation by a minor structural adjustment. Thus, the substitution (SeO_3) $\leftrightarrow$ (PO_4) coupled with the substitution OW(29) $\leftrightarrow$ O(22) may not disrupt the structural connectivity of phurcalite, but experimental verification of this substitution is necessary.

In the structure of phosphuranylite [73], the apical anions of the phosphate tetrahedra are invariably bonded to U^{6+} in the interlayer with a bond-valence of approximately 0.67 vu calculated using the bond-valence parameters provided by Burns et al. [52]. Such a high bond-valence requirement cannot be satisfied by the oxygen anions of the H_2O groups. Therefore, the substitution (SeO_3) $\leftrightarrow$ (PO_4) in phosphuranylite will have serious structural consequences and is unlikely to occur.

The substitution of selenate into the sheets of uranyl phosphate minerals is unlikely to occur because this would necessitate the sharing of an edge between a uranyl polyhedron and a selenate tetrahedron.

4.3.4. Uranyl carbonates

The close similarity between the sheets in the structures of rutherfordine and [(UO_2)(SeO_3)] (Fig. 7(a)) implies that the substitution (SeO_3) $\leftrightarrow$ (CO_3) can occur

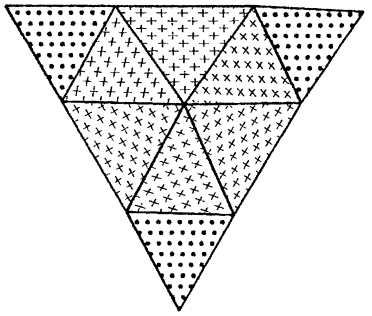

Fig. 11. The uranyl carbonate cluster that is the basis of several uranyl carbonate minerals. The uranyl polyhedron is shaded with crosses, and the carbonate triangles are stippled.

in the structure of rutherfordine, and possibly other uranyl carbonates. Most uranyl carbonates have structures that are based upon finite clusters of composition $(UO_2)(CO_3)_3$ (Fig. 11). These clusters are linked to cation polyhedra of lower bond-valence to form several mineral structures. The substitution of (SeO_3) for (CO_3) in structures does not require a charge-balancing mechanism, thus it depends primarily on the geometry of the two polyhedra. The edge-length of a selenite polyhedron is ~0.255 to 0.266 nm (see above); whereas, a typical carbonate triangle has an edge-length of ~0.22 nm. This edge-length mismatch is small enough that significant substitution of selenite should occur in many uranyl carbonates.

5. Concluding remarks

(1) Under the Eh–pH conditions that are expected to occur during the oxidative alteration of spent nuclear fuel, selenite or selenate is predicted to be the dominant species of aqueous selenium.

(2) Selenium concentrations in the near-field of nuclear waste repositories may be much higher than that in ordinary and even selenium-affected natural systems. If the upper limit of the selenium concentration in the near-field is determined by the solubilities of metal-selenites, the calculated selenium concentrations are a function of pH with their minimums being 3.94×10^{-4} m with respect to $CaSeO_3$, 6.31×10^{-4} m with respect to $MgSeO_3$ and 4.54×10^{-3} m with respect to $Fe_2(OH)_4SeO_3$, assuming that the concentrations of Ca^{2+}, Mg^{2+} and Fe^{3+} in the near-field solutions are equal to those in J-13 groundwater at Yucca Mountain. As compared with the 10 μg/l (1.27×10^{-7} m) and 400 μg/l (5.06×10^{-6} m) selenium concentrations permitted in drinking and waste water, respectively [28] and considering the radiotoxicity of ^{79}Se, the metal-selenite solubility-limited ^{79}Se concentrations are high.

(3) Adsorption of selenite by backfill and geological materials is significant in acidic solutions but decreases sharply as the pH increases. In the alkaline environments that are expected in the near-field due to reaction with concrete [50,51]; thus the mobility of selenite will not be reduced significantly by adsorption.

(4) Because large amounts of uranyl phases are expected to form during the oxidative dissolution of spent nuclear fuel, the mobility of selenium can be greatly reduced if it is incorporated into the secondary uranyl phases as an impurity. The possible incorporation of (SeO_3) into the structures of selected uranyl silicates and phosphates is summarized in Table 4. (SeO_3) may substitute for (SiO_3OH) in structures of α-uranophane and boltwoodite that are expected to be the dominant alteration phases of UO_2 in Si-rich groundwater. The substitutions $(SeO_3) \leftrightarrow (SiO_4)$ in sklodowskite, $Mg[(UO_2)(SiO_3OH)]_2(H_2O)$, and $(SeO_3) \leftrightarrow (PO_4)$ in phurcalite, $Ca_2[(UO_2)_3(PO_4)_2O_2](H_2O)_7$, may occur, but this must be verified by experimental investigations. The

Table 4
Summary of the possible substitutions of (SiO_3OH), (SiO_4) and (PO_4) by (SeO_3) in the selected uranyl phases

Group	Mineral	Formula	Species [a]	Bond-valence [b]	Substitution
SiO_3OH	α-uranophane	$Ca[(UO_2)(SiO_3OH)]_2(H_2O)_5$	H_2O	H-bond	likely
			Ca	0.29	probable
	sklodowskite	$Mg[(UO_2)(SiO_3OH)]_2(H_2O)_6$	Mg	0.31	probable
	boltwoodite	$(K,Na)[(UO_2)(SiO_3OH)]$	H_2O	H-bond	likely
		$(H_2O)_{1.5}$	K	0.048	likely
SiO_4	soddyite	$(UO_2)_2(SiO_4)(H_2O)_2$	$U\phi_5$	0.56	unlikely
PO_4	phurcalite	$Ca_2[(UO_2)_3(PO_4)_2O_2](H_2O)_7$	Ca	0.33	probable
			Ca	0.46	unlikely
	phosphuranylite	$KCa(H_3O)_3(UO_2)[(UO_2)_3$ $(PO_4)_2O_2]_2(H_2O)_8$	$U\phi_4$	0.67	unlikely

[a] Chemical species connected to the apical anion that will be eliminated due to the substitution.
[b] Refer to the bond-valence between the apical anion that will be eliminated due to the substitution and the chemical species.

close similarity between the sheets in the structures of rutherfordine and $[(UO_2)(SeO_3)]$ implies that the substitution $(SeO_3) \leftrightarrow (CO_3)$ can occur. However, the substitutions $(SeO_3) \leftrightarrow (SiO_3OH)$ in soddyite and $(SeO_3) \leftrightarrow (PO_4)$ in phosphuranylite will disrupt the structural connectivity and are unlikely to occur. The polyhedra that contain cations with the valence 6+ (with the exception of U^{6+}) seldom share an edge with a uranyl polyhedra, while each of the silicate tetrahedra and phosphate tetrahedra in the structures of α-uranophane, boltwoodite, sklodowskite, soddyite and phurcalite, respectively, involves the sharing of an edge with a uranyl polyhedron. As such, the substitution of selenate for silicate or phosphate in any of these structures is unlikely.

(5) The incorporation mechanism conclusions are based on crystal–chemical arguments only, and experimental verification is required, especially for the incorporation of (SeO_3) into sklodowskite and phurcalite.

Acknowledgements

This research was funded by the Environmental Management Sciences Program of the United States Department of Energy [DE-FG07-97ER-14816 (RCE) and DE-FG07-97ER14820 (PCB)].

References

[1] H.W. Lakin, in: H.L. Cannon, H.C. Hopps (Eds.), Geochemical Environment in Relation to Health and Disease, Special Paper, 140, Geological Society of America, Boulder, CO, 1972, p. 27.
[2] National Academy of Science, Food and Nutrition Board Selenium and Human Health Nutrition Reviews, Washington D.C. vol. 34, 1976, p. 247.
[3] T.W. Melnyk, J. McMurry, F.P. Sargent, Proceedings of the 1994 American Nuclear Society International High-Level Radioactive Waste Management Conference, Las Vegas, Nevada 3 (1994) 1222.
[4] Civilian Radioactive Waste Management System Management and Operating Contractor, Total System Performance Assessment – 1995: An Evaluation of the Potential Yucca Mountain Repository prepared by TRW Environmental Safety Systems, 1995.
[5] J.H. Kessler et al., Biosphere modeling and dose assessment for Yucca Mountain. Final Report TR – 107190 3294-18 Electric Power Research Institute prepared by QuantiSci, 1996.
[6] S. Jiang, J. Duo, Sh. Jiang, C. Li, Sh. Jiang, A. Cui, M. He, S. Wu, S. Li, Nucl. Instrum. Meth. B123 (1997) 405.
[7] R.S. Forsyth, L.O. Werme, J. Nucl. Mater. 190 (1992) 3.
[8] L.H. Johnson, L.O. Werme, Mater. Res. Soc. Bull. (1994) 24.
[9] D.J. Wronkiewicz, J.K. Bates, T.J. Gerding, E. Veleckis, J. Nucl. Mater. 190 (1992) 107.
[10] D.J. Wronkiewicz, J.K. Bates, S.F. Wolf, E.C. Buck, J. Nucl. Mater. 238 (1996) 78.
[11] P.A. Finn, J.C. Hoh, S.F. Wolf, S.A. Slater, J.K. Bates, Radiochim. Acta 74 (1996) 65.
[12] E.C. Buck, R.J. Finch, P.A. Finn, J.K. Bates, in: I.G McKinley (Ed.), Mater. Res. Soc. Symp. Proc. 506 (1998) 87.
[13] P.C. Burns, R.C. Ewing, M.L. Miller, J. Nucl. Mater. 245 (1997) 1.
[14] F. Chen, P.C. Burns, R.C. Ewing, Near-field behavior of technetium during the dissolution of spent nuclear fuel, J. Nucl. Mater. (submitted).
[15] S. Sunder, D.W. Shoesmith, M.G. Balley, F.W. Stanchell, N.S. Mcintyre, J. Electroanalyt. Chem. 130 (1981) 163.
[16] D.W. Shoesmith, S. Sunder, J. Nucl. Mater. 190 (1992) 20.
[17] R.J. Finch, R.C. Ewing, J. Nucl. Mater. 190 (1992) 33.
[18] D. Langmuir, Geochim. Cosmochim. Acta 42 (1978) 547.
[19] E.C. Pearcy, J.D. Prikryl, W.M. Murphy, B.W. Leslie, Appl. Geochem. 9 (1994) 713.
[20] C.J. Bruton, and H.F. Shaw, in: M.J. Apted, R.E Westerman (Ed.), Mater. Res. Soc. Symp. Proc. 112 (1988) 485.
[21] R.A. Freeze, J.A. Cherry, Groundwater, Prentice-Hall, Englewood Cliffs, 1979, pp. 268–289.
[22] I. Grenthe, J. Fuger, R.J.M. Konings, R.J. Lemire, A.B. Muller, C. Nguyen-Trung, H. Wanner, Chemical Thermodynamics of Uranium, North-Holland, Amsterdam, vol. 99, p. 73.
[23] F. Chen, R.C. Ewing, S.B. Clark, Am. Mineral. 84 (1999) 650.
[24] Y. Fujikawa, M. Fukui, Radiochim. Acta 76 (1997) 163.
[25] M.A. Elrashidi, D.C. Adriano, S.M. Workman, W.L. Lindsay, Soil Sci. 144 (1987) 141.
[26] M.E. Essington, Soil Sci. Soc. Am. J. 52 (1988) 1574.
[27] S. Sharmasarkar, K.J. Reddy, G.F. Vance, Chem. Geol. 132 (1996) 165.
[28] S.J. Deverel, R.J. Gilliom, R. Fugii, J.A. Izbicki, J.C. Fields, US Geol. Surv. Report 84-4319, 1984.
[29] D.D. Wagman, W.H. Evans, V.B. Parker, R.H. Schumm, I. Halow, S.M. Bailey, K.L. Churney, R.L. Buttall, J. Phys. Chem. Ref. Data 11, Suppl. 2 (1982) 392.
[30] F.J. Hingston, A.M. Posner, J.P. Quirk, Adv. Chem., No. 79, Washington DC, 1968, p. 82.
[31] R.L. Parfitt, Adv. Agronomy 30 (1978) 1.
[32] S. Goldberg, G. Sposito, Soil Sci. Soc. Am. J. 48 (1984) 722.
[33] K.F. Hayes, A.L. Roe, G.E. Brown Jr., K.O. Hodgson, G.A. Parks, Science 238 (1987) 783.
[34] M.J. Blaylock, T.A. Tawfic, G.F. Vance, Soil Sci. 159 (1995) 43.
[35] M.M. Benjamin, N.S. Bloom, In P.H. Tewari (Ed.), Adsorption from Aqueous Solutions, Plenum, New York, 1981, p. 41.
[36] J.A. Davis, J.O. Leckie, J. Colloid Interf. Sci. 74 (1980) 32.
[37] M.K. John, W.M.H. Saunders, J.H. Watkinson, New Zealand J. Agriculture Res. 19 (1976) 143.
[38] A.A. Hamdy, G. Gissel-Nielsen, Z. Pflanzenernaehr. Bodenkd. 140 (1977) 63.
[39] B. Bar-Yosef, D. Meek, Soil Sci. 144 (1987) 11.
[40] S.S.S. Rajan, J. Soil Sci. 30 (1979) 709.
[41] H.H. Neal, G. Sposito, K.M. Holtzclaw, S.J. Traina, Soil Sci. Soc. Am. J. 51 (1987) 1161.

[42] R.H. Neal, G. Sposito, K.M. Holtzclaw, S.J. Traina, Soil Sci. Soc. Am. J. 51 (1987) 1165.
[43] S. Goldberg, Soil Sci. Soc. Am. J. 49 (1985) 851.
[44] P.H. Masscheleyn, R.D. Delaune, W.H. Patrick Jr., J. Environ. Quality 20 (1991) 522.
[45] L.S. Balistrieri, T.T. Chao, Soil Sci. Soc. Am. J. 51 (1987) 1145.
[46] B. Bar-Yosef, U. Kafkafi, N. Lahav, Soil Sci. Soc. Am. J. Proc. 33 (1969) 672.
[47] R. Keren, R.G. Gast, B. Bar-Yosef, Soil Sci. Soc. Am. J. 45 (1981) 45.
[48] H.R. Geering, E.E. Gray, L.H.P. Jone, W.H. Allaway, Soil Sci. Soc. Am. Proc. 32 (1968) 35.
[49] R.D. Harter, Soil Sci. Soc. Am. J. 48 (1984) 749.
[50] J. Eikenberg, P.C. Lichtner, in: Y.K. Kharaka, A. Maest (Ed.), Proceedings of Seventh International Symposium on Water–Rock Interaction, vol. 1, Rotterdam, Netherlands, 1999, p. 377.
[51] W.M. Murphy, R.T. Pabalan, Geochemical Investigations Related to the Yucca Mountain Environment and Potential Nuclear Waste Repository. NUREG/CR-6288, Washington DC: US Nuclear Regulatory Commission, 277032, 1994.
[52] P.C. Burns, R.C. Ewing, F.C. Hawthorne, Can. Mineral. 35 (1997) 1551.
[53] P.C. Burns, M.L. Miller, R.C. Ewing, Can. Mineral. 34 (1996) 845.
[54] R.D. Shannon, Acta Crystallogr. A32 (1976) 751.
[55] M.A. Cooper, F.C. Hawthorne, Can. Mineral. 33 (1995) 1103.
[56] D. Ginderow, F. Cesbron, Acta Crystallogr. C39 (1983) 824.
[57] D. Ginderow, F. Cesbron, Acta Crystallogr. C39 (1983) 1605.
[58] R. Vochten, N. Blaton, O. Peeters, M. Deliens, Can. Mineral. 34 (1996) 1317.
[59] B.O. Loopstra, N.P. Brandenberg, Acta Crystallogr. B34 (1978) 1335.
[60] C.L. Christ, J.R. Clark, H.T. Evans Jr., Science 121 (1955) 472.
[61] V.E. Mistryukov, Y.N. Michailov, Coord. Chem. (USSR), 9, 1983, 97 (in Russian).
[62] N.P. Brandenberg, B.O. Loopstra, Acta Crystallogr. B34 (1978) 3734.
[63] V.N. Serezhkin, M.A. Soldakina, V.A. Efremov, Zh. Struktur. Khim. 22 (1981) 171.
[64] V.A. Blatov, L.B. Serezhkina, V.N. Serzhkin, V.K. Trunov, Russian J. Inorg. Chem. 34 (1989) 91.
[65] J.C. Trombe, A. Gleizes, J. Glay, Acta Crystallogr. C41 (1985) 1571.
[66] M. Koskenlinna, J. Valkonen, Acta Crystallogr. C5 (1996) 1857.
[67] D. Ginderow, Acta Crystallogr. C44 (1988) 421.
[68] R.R. Ryan, A. Rosenzweig, Crystal Structure Commun. 6 (1977) 611.
[69] F.V. Stohl, D.K. Smith, Amer. Mineral. 66 (1981) 610.
[70] A. Rosenzweig, R.R. Ryan, Crystal Structure Commun. 6 (1977) 617.
[71] F. Demartin, C.M. Gramaccioli, T. Pilati, Acta Crystallogr. C48 (1992) 1.
[72] Y.S. Makarov, V.I. Ivanov, Dokl. Acad. Sci. USSR, Earth Sci. Sec. 132 (1960) 601.
[73] F. Demartin, V. Diella, S. Donzelli, C.M. Gramaccioli, T. Pilati, Acta Crystallogr. B47 (1991) 439.
[74] D. Atencio, R. Neumann, A.J.G.C. Silva, Y.P. Mascarenhas, Can. Mineral. 29 (1991) 95.
[75] P. Piret, J. Piret-Meunier, Bull. Minéral. 111 (1988) 439.
[76] P. Piret, J. Piret-Meunier, M. Deliens, Eur. J. Miner. 2 (1990) 399.
[77] P. Piret, J.P. Declercq, Bull. Minér. 106 (1983) 383.
[78] P. Piret, M. Deliens, J. Piret-Meunier, Bull. Minér. 111 (1988) 443.
[79] P. Piret, J. Piret-Meunier, J.-P. Declercq, Acta Crystallogr. B35 (1979) 1880.
[80] P. Piret, M. Deliens, Bull. Minér. 110 (1987) 65.
[81] C. Frondel, Systematic Mineralogy of Uranium and Thorium. US Geological Survey Bulletin 1064, Washington, DC, US Government Printing Office, 1958.
[82] T. Wadsten, J. Nucl. Mater. 64 (1977) 315.
[83] C.N. Wilson, Results from NNWSI Series 3 Spent Fuel Dissolution Tests, Pacific Northwest Laboratory Report PNL-7170, Richland, 1990.
[84] P.C. Burns, Can. Mineral. 36 (1998) 1061.
[85] P.C. Burns, Can. Mineral. 36 (1998) 1069.
[86] A.A. Chernikov, D.P. Shaskin, I.N. Gravilova, Dokl. Akad. Nauk SSSR 2 (1975) 144 (in Russian).
[87] F.C. Hawthorne, Z. Kristallogr. 201 (1992) 183.